

Polarized and unpolarized nucleon structure functions from lattice QCD

M. Göckeler,^{1,2} R. Horsley,^{1,3} E.-M. Ilgenfritz,³ H. Perlt,⁴ P. Rakow,⁵ G. Schierholz,^{6,1} and A. Schiller⁴

¹Gruppe Theorie der Elementarteilchen, Höchstleistungsrechenzentrum HLRZ, c/o Forschungszentrum Jülich, D-52425 Jülich, Germany

²Institut für Theoretische Physik, RWTH Aachen, D-52056 Aachen, Germany

³Institut für Physik, Humboldt-Universität, D-10115 Berlin, Germany

⁴Fakultät für Physik und Geowissenschaften, Universität Leipzig, D-04109 Leipzig, Germany

⁵Institut für Theoretische Physik, Freie Universität, D-14195 Berlin, Germany

⁶Deutsches Elektronen-Synchrotron DESY, D-22603 Hamburg, Germany

(Received 11 September 1995)

We report on a high statistics quenched lattice QCD calculation of the deep-inelastic structure functions F_1 , F_2 , g_1 , and g_2 of the proton and neutron. The theoretical basis for the calculation is the operator product expansion. We consider the moments of the leading twist operators up to spin four. Using Wilson fermions the calculation is done for three values of κ , and we perform the extrapolation to the chiral limit. The renormalization constants, which lead us from lattice to continuum operators, are calculated in perturbation theory to one loop order.

PACS number(s): 12.38.Gc, 13.85.Hd, 13.88.+e

I. INTRODUCTION

Deep-inelastic lepton-nucleon scattering is described by four structure functions: F_1 , F_2 , g_1 , and g_2 . The spin-averaged structure functions F_1 and F_2 carry information about the overall density of quarks and gluons in the nucleon. They have played a seminal role in the development of our current understanding of the structure of hadrons. The polarized structure function g_1 goes one step further and probes the distribution of quarks of a given helicity in the longitudinally polarized nucleon. Recent measurements of g_1 [1] have revealed the (at first sight) surprising result that only a small fraction of the nucleon's spin is carried by quarks. This has triggered a great deal of interest in the subject. The other polarized structure function g_2 has no interpretation in purely partonic language. It involves a twist-three operator and thus offers the first direct measurement of higher twist operator matrix elements [2]. Experiments that measure g_2 are currently being performed at DESY and SLAC.

We have initiated a program to compute F_1 , F_2 , g_1 , and g_2 on the lattice [3]. For an earlier attempt to compute the unpolarized structure functions see [4]. The theoretical basis for such a calculation is the operator product expansion (OPE), which relates the moments of the structure functions to forward nucleon matrix elements of certain local operators. Where a parton model interpretation exists, it can be mapped onto an OPE analysis. Our calculation will be in the quenched approximation, where internal quark loops are neglected. In this paper we shall also neglect gluonic operators, which contribute only to higher order in the coupling constant expansion. For the unpolarized structure functions we then have, for the leading twist contribution,

$$2 \int_0^1 dx x^{n-1} F_1(x, Q^2) = \sum_{f=u,d} c_{1,n}^{(f)}(\mu^2/Q^2, g(\mu)) v_n^{(f)}(\mu),$$

$$\int_0^1 dx x^{n-2} F_2(x, Q^2) = \sum_{f=u,d} c_{2,n}^{(f)}(\mu^2/Q^2, g(\mu)) v_n^{(f)}(\mu),$$

(1) for even n and $n \geq 0$ ($n \geq 2$) for g_1 (g_2), where [2]

for $n \geq 2$ (generally even n), where

$$\frac{1}{2} \sum_s \langle \vec{p}, \vec{s} | \mathcal{O}_{\{\mu_1 \dots \mu_n\}}^{(f)} | \vec{p}, \vec{s} \rangle = 2 v_n^{(f)} [p_{\mu_1} \dots p_{\mu_n} - \text{traces}],$$

$$\mathcal{O}_{\mu_1 \dots \mu_n}^{(f)} = \left(\frac{i}{2} \right)^{n-1} \bar{\psi} \gamma_{\mu_1} \vec{D}_{\mu_2} \dots \vec{D}_{\mu_n} \psi - \text{traces} \quad (2)$$

with $\psi = u(d)$ for $f = u(d)$, and

$$c_{1,n}^{(f)}(\mu^2/Q^2, g(\mu)) = Q^{(f)2} [1 + g(\mu)^2 \bar{c}_{1,n}(\mu^2/Q^2, g(\mu))],$$

$$c_{2,n}^{(f)}(\mu^2/Q^2, g(\mu)) = Q^{(f)2} [1 + g(\mu)^2 \bar{c}_{2,n}(\mu^2/Q^2, g(\mu))]. \quad (3)$$

Here μ denotes the subtraction point, and $\{\dots\}$ indicates symmetrization. We have chosen the normalization $\langle \vec{p}, \vec{s} | \vec{p}', \vec{s}' \rangle = (2\pi)^3 2E_p \delta(\vec{p} - \vec{p}') \delta_{s,s'}$, $s^2 = -m_N^2$. The moments of F_1 , F_2 have the parton model interpretation

$$v_n^{(f)} = \langle x^{n-1} \rangle^{(f)}, \quad (4)$$

where x is the fraction of the nucleon momentum carried by the quarks. In the quenched approximation the above-mentioned equations hold for odd n as well.

For the polarized structure functions we have, again for the leading twist contribution,

$$2 \int_0^1 dx x^n g_1(x, Q^2) = \frac{1}{2} \sum_{f=u,d} e_{1,n}^{(f)}(\mu^2/Q^2, g(\mu)) a_n^{(f)}(\mu), \quad (5)$$

$$2 \int_0^1 dx x^n g_2(x, Q^2) = \frac{1}{2} \frac{n}{n+1} \sum_{f=u,d} [e_{2,n}^{(f)}(\mu^2/Q^2, g(\mu)) \times d_n^{(f)}(\mu) - e_{1,n}^{(f)}(\mu^2/Q^2, g(\mu)) \times a_n^{(f)}(\mu)], \quad (6)$$

$$\begin{aligned} \langle \vec{p}, \vec{s} | \mathcal{O}_{\{\sigma\mu_1 \dots \mu_n\}}^{5(f)} | \vec{p}, \vec{s} \rangle &= \frac{1}{n+1} a_n^{(f)} [s_\sigma p_{\mu_1} \dots p_{\mu_n} + \dots \\ &\quad - \text{traces}], \\ \langle \vec{p}, \vec{s} | \mathcal{O}_{[\sigma\{\mu_1\} \dots \mu_n]}^{5(f)} | \vec{p}, \vec{s} \rangle &= \frac{1}{n+1} d_n^{(f)} [(s_\sigma p_{\mu_1} - s_{\mu_1} p_\sigma) \\ &\quad \times p_{\mu_2} \dots p_{\mu_n} + \dots - \text{traces}], \end{aligned} \quad (7)$$

$$\mathcal{O}_{\sigma\mu_1 \dots \mu_n}^{5(f)} = \left(\frac{i}{2}\right)^n \bar{\psi} \gamma_\sigma \gamma_5 \vec{D}_{\mu_1} \dots \vec{D}_{\mu_n} \psi - \text{traces},$$

and

$$\begin{aligned} e_{1,n}^{(f)}(\mu^2/Q^2, g(\mu)) &= Q^{(f)2} [1 + g(\mu)^2 \bar{e}_{1,n}(\mu^2/Q^2, g(\mu))], \\ e_{2,n}^{(f)}(\mu^2/Q^2, g(\mu)) &= Q^{(f)2} [1 + g(\mu)^2 \bar{e}_{2,n}(\mu^2/Q^2, g(\mu))]. \end{aligned} \quad (8)$$

In Eq. (7) $[\dots]$ indicates antisymmetrization. In parton model language,

$$a_0^{(u)} = 2\Delta u, \quad a_0^{(d)} = 2\Delta d, \quad (9)$$

where $\Delta u, \Delta d$ determine the fraction of the nucleon spin that is carried by the quarks. A similar interpretation holds for the higher spin operators. The structure function g_2 consists of two contributions: $a_n^{(f)}$ is the so-called Wandzura-Wilczek contribution [5] which corresponds to twist two, whereas $d_n^{(f)}$ corresponds to twist three. In addition to $d_n^{(f)}$ there is a contribution to g_2 from a twist-three operator which is proportional to the quark mass [6]. Since we are mainly interested in the chiral limit we have neglected that.

II. LATTICE CALCULATION

We perform our quenched QCD calculations for Wilson fermions with $r=1$ on a $16^3 \times 32$ lattice. For the gauge coupling we take $\beta \equiv 6/g^2 = 6.0$. To be able to extrapolate our results to the chiral limit, we run at three different hopping parameters, $\kappa = 0.155, 0.153, \text{ and } 0.1515$. This corresponds to physical quark masses m_q of roughly 70, 130, and 190 MeV, respectively, using the perturbative relation

$$m_q a = 0.56 \left(\frac{1}{\kappa} - \frac{1}{\kappa_c} \right), \quad (10)$$

where a is the lattice spacing.

For the gauge update we use a cycle consisting of a single three-hit Metropolis sweep followed by 16 overrelaxation sweeps [7]. We repeat this cycle 50 times in order to generate a new configuration. The resulting configurations seem to be independent. We see no correlations between hadronic quantities calculated on different gauge field configurations. The calculations are carried out on Quadrics Q16 and QH2 parallel computers. For details of the implementation of our code on these machines see [3]. So far we have collected of the order 1000, 600, and 400 independent configurations at the three κ values.

To calculate the nucleon matrix elements we first compute two- and three-point correlation functions defined by

$$\begin{aligned} C_\Gamma(t, \vec{p}) &= \sum_{\alpha, \beta} \Gamma_{\beta, \alpha} \langle B_\alpha(t, \vec{p}) \bar{B}_\beta(0, \vec{p}) \rangle, \\ C_\Gamma(t, \tau, \vec{p}, \mathcal{O}) &= \sum_{\alpha, \beta} \Gamma_{\beta, \alpha} \langle B_\alpha(t, \vec{p}) \mathcal{O}(\tau) \bar{B}_\beta(0, \vec{p}) \rangle. \end{aligned} \quad (11)$$

The lattice operators \mathcal{O} used here are obtained from the operators in the Euclidean continuum, which look exactly like the operators in Eqs. (2) and (7) up to factors of i , by replacing the covariant derivative by the lattice covariant derivative so that \vec{D}_μ becomes

$$\vec{D}_\mu(x, y) = \frac{1}{2} [U_\mu(x) \delta_{y, x+\hat{\mu}} - U_\mu^\dagger(x-\hat{\mu}) \delta_{y, x-\hat{\mu}}]. \quad (12)$$

We write the ratio of three- to two-point correlation functions as

$$\begin{aligned} R(t, \tau, \vec{p}, \Gamma, \mathcal{O}) &= C_\Gamma(t, \tau, \vec{p}, \mathcal{O}) / C_{\frac{1}{2}(1+\gamma_4)}(t, \vec{p}) \\ &= \frac{1}{2\kappa} \frac{E_p^-}{E_p^- + m_N} F(\Gamma, \mathcal{J}) \end{aligned} \quad (13)$$

(for $0 \ll \tau \ll t$) with

$$\begin{aligned} F(\Gamma, \mathcal{J}) &= \frac{1}{4} \text{Tr}[\Gamma N \mathcal{J} N], \\ N &= \gamma_4 - i\vec{p} \cdot \vec{\gamma} / E_p^- + m_N / E_p^-, \end{aligned} \quad (14)$$

and \mathcal{J} defined by

$$\langle \vec{p}, \vec{s} | \mathcal{O} | \vec{p}, \vec{s} \rangle = \bar{u}(\vec{p}, \vec{s}) \mathcal{J} u(\vec{p}, \vec{s}). \quad (15)$$

When calculating three-point functions it is particularly important that the baryon operator B has only little overlap with excited baryon states, in order to make the plateau region in τ as broad as possible. As our basic proton operator we use (with $C = \gamma_4 \gamma_2$ in our representation)

$$B_\alpha(t, \vec{p}) = \sum_{x, a, b, c} e^{-i\vec{p} \cdot \vec{x}} \epsilon_{abc} u_\alpha^a(x) [u^b(x) C \gamma_5 d^c(x)] \quad (16)$$

with two important improvements. First we use ‘‘Jacobi smearing’’ [8] (a version of [9]) in order to have an extended proton operator. Thus each quark operator in Eq. (11) is replaced by

$$\psi \rightarrow \psi^S = \sum_{n=0}^{N_s} (\kappa_s \vec{D})^n \psi, \quad (17)$$

and similarly for $\bar{\psi}$ as we smear both source and sink. We found suitable values of the parameters to be $N_s = 50, \kappa_s = 0.21$, which for our largest κ value gave a rms radius of about 4, corresponding roughly to 0.5 fm, i.e., half the nucleon radius. Second we replace each spinor by

$$\psi \rightarrow \psi^{\text{NR}} = \frac{1}{2} (1 + \gamma_4) \psi, \quad \bar{\psi} \rightarrow \bar{\psi}^{\text{NR}} = \bar{\psi} \frac{1}{2} (1 + \gamma_4). \quad (18)$$

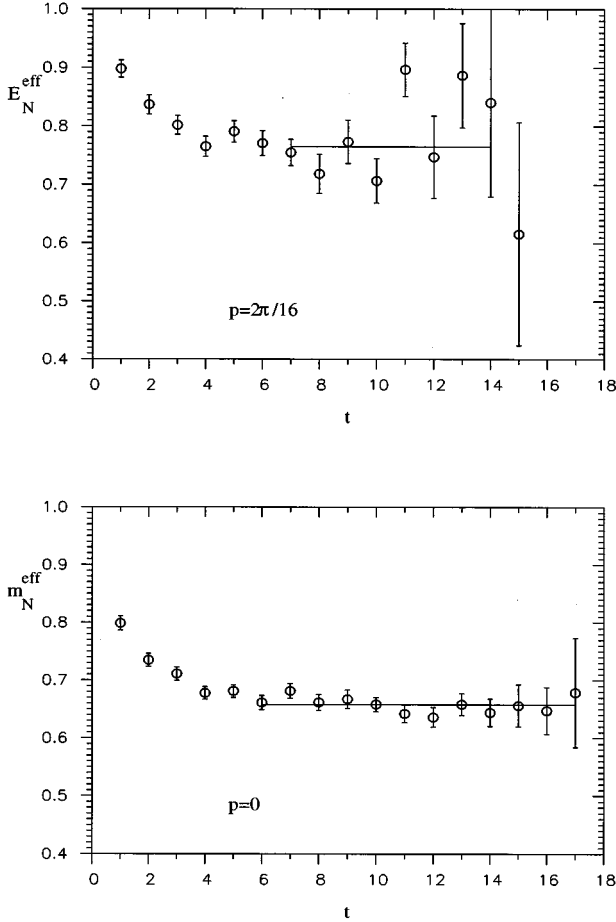


FIG. 1. Effective nucleon mass plot for $\vec{p}=0$ (bottom), and effective nucleon energy plot for $|\vec{p}|=2\pi/16$ (top) at $\kappa=0.155$. Both source and sink are smeared. The horizontal lines indicate the result of the fit as well as the fit interval.

This replacement leaves quantum numbers unchanged, but we expect it to improve overlap with those baryons which have slow-moving valence quarks. Practically this means that for each baryon propagator we invert on a smeared local source and consider only the first two Dirac components. So we only have 2×3 inversions to perform rather than the usual 4×3 inversions, which saves a factor 2 in computer time in the inversion.

In Ref. [3] we have seen that the projection (18) is particularly effective at reducing unwanted backward propagating states, which extends the window that one can practically use for matrix element calculations to well above half the temporal extent of the lattice. In Fig. 1 we show a plot of the resulting effective nucleon energy, as given by $\ln[C(t)/C(t+1)]$, for $\vec{p}=0$ and $|\vec{p}|=2\pi/16$ at our smallest quark mass. For zero nucleon momentum we find a good plateau with a proton mass of 0.658(5). For the lowest non-zero momentum we find an energy of 0.765(11), which is in good agreement with the continuum dispersion relation. In both cases we see that after a distance of about four time units there is very little trace of an excited state. In Table I we give the mass values of the nucleon together with those of the π and ρ for our three values of κ . Note that at the smallest quark mass the ratio m_π/m_ρ is about 0.7. The chiral

TABLE I. The hadron masses in lattice units at $\beta=6.0$.

	κ		
	0.1515	0.153	0.155
m_π	0.504(2)	0.422(2)	0.297(2)
m_ρ	0.570(2)	0.507(2)	0.422(2)
m_N	0.900(5)	0.798(5)	0.658(5)

limit is obtained by extrapolating in $1/\kappa$ to zero π mass. Assuming, as usual, that m_π^2 depends linearly on $1/\kappa$, we obtain from our data the critical value $\kappa_c=0.15693(4)$. In Fig. 2 we plot m_π^2 , m_ρ^2 , and m_N^2 as a function of $1/\kappa$. In this plot we have also included other recent results at $\beta=6.0$. A combined fit gives $m_N/m_\rho=1.37$ in the chiral limit. We have tried linear fits to the nucleon and ρ masses as well. However, the fits were not acceptable. The same observation was made in Ref. [13].

To calculate three-point functions we require additional propagators, one for each chosen t , \vec{p} , and Γ . We have fixed t at 13 and have chosen $\Gamma=\frac{1}{2}(1+\gamma_4)$, corresponding to the unpolarized case, and $\Gamma=\frac{1}{2}(1+\gamma_4)i\gamma_5\gamma_2$, corresponding to polarization (+ - -) in the two-direction. For the momentum we have taken $\vec{p}=0$ and $\vec{p}=(2\pi/16,0,0)\equiv(p_1,0,0)$. We have also considered $\psi=u, d$ separately. This means that we must find $2 \times 2 \times 2=8$ (half) quark propagators. The choice $t=13$ is sufficient. Larger values of t lead to unacceptably large errors in the signal for R . Test runs for $t=17$ turned out to have errors of ~ 2 larger, which roughly corresponds to

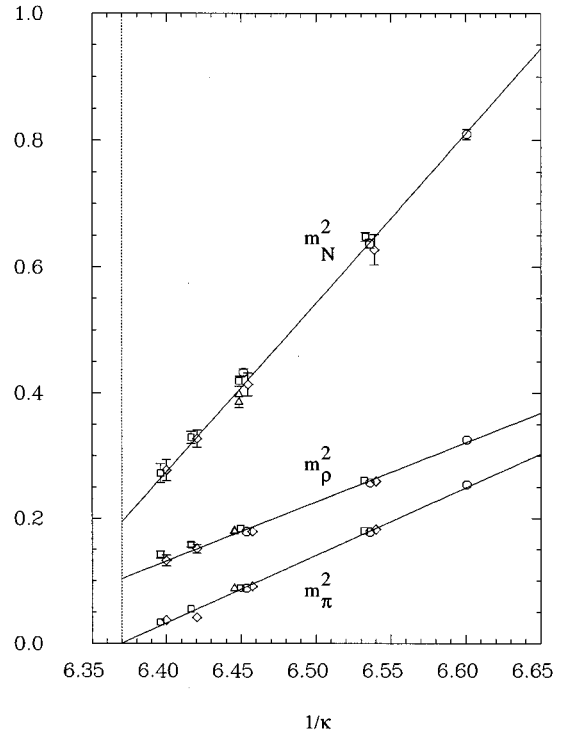
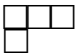
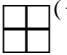


FIG. 2. m_π^2 , m_ρ^2 , and m_N^2 as a function of $1/\kappa$ together with other recent results of the literature: \circ this work, \square Ref. [10], \diamond Ref. [11], \triangle Ref. [12]. The fit to all data points combined gives $\kappa_c=0.15699(5)$.

TABLE II. The lattice operators and their representation. The momentum is taken to be $\vec{p} = (2\pi/16, 0, 0) \equiv (p_1, 0, 0)$ in the case of $v_{2,a}, v_3, v_4, a_2, d_2$, and $\vec{p} = 0$ elsewhere. C denotes charge conjugation.

$\langle \mathcal{O} \rangle$	Components	Representation		C
		Ref. [14]	Ref. [15]	
$v_{2,a}$	$\mathcal{O}_{\{14\}}$	$\tau_3^{(6)}$	$6^{(+)}$	+
$v_{2,b}$	$\mathcal{O}_{\{44\}} - \frac{1}{3}(\mathcal{O}_{\{11\}} + \mathcal{O}_{\{22\}} + \mathcal{O}_{\{33\}})$	$\tau_1^{(3)}$	 (+)	+
v_3	$\mathcal{O}_{\{114\}} - \frac{1}{2}(\mathcal{O}_{\{224\}} + \mathcal{O}_{\{334\}})$	$\tau_1^{(8)}$	$8^{(+)}$	-
v_4	$\mathcal{O}_{\{1144\}} + \mathcal{O}_{\{2233\}} - \mathcal{O}_{\{1133\}} - \mathcal{O}_{\{2244\}}$	$\tau_1^{(2)}$	 (+)	+
a_0	\mathcal{O}_2^5	$\tau_4^{(4)}$	$(\frac{1}{2}, \frac{1}{2})^{(-)}$	+
a_2	$\mathcal{O}_{\{214\}}^5$	$\tau_3^{(4)}$	$(\frac{1}{2}, \frac{1}{2})^{(+)}$	+
d_2	$\mathcal{O}_{\{2[1]4\}}^5$	$\tau_1^{(8)}$	$8^{(+)}$	+

the increase in the noise in the baryon correlation function from $t = 13$ to $t = 17$.

III. LATTICE OPERATORS AND THEIR RENORMALIZATION

The bare lattice operators $\mathcal{O}(a)$ are in general divergent. We define finite operators $\mathcal{O}(\mu)$, renormalized at the scale μ , by

$$\mathcal{O}(\mu) = Z_{\mathcal{O}}((a\mu)^2, g(a))\mathcal{O}(a), \quad (19)$$

where

$$\langle q(p) | \mathcal{O}(\mu) | q(p) \rangle = \langle q(p) | \mathcal{O}(a) | q(p) \rangle \Big|_{p^2 = \mu^2}^{\text{tree}} \quad (20)$$

with $|q(p)\rangle$ being a quark state of momentum p . In the limit $a \rightarrow 0$ this definition amounts to the continuum, momentum subtraction renormalization scheme.

The lattice operators transform under the discrete hypercubic group $H(4)$ [14,15]. They must be constructed such that they belong to a definite irreducible representation of the latter. In particular they must not mix with lower-dimensional operators. This is prerequisite to the operators being multiplicatively renormalizable. Furthermore, from the more practical point of view, the operators should only require a nonzero spatial momentum in at most one direction. We have considered the operators listed in Table II. For the group theoretical classification of the lattice operators see Ref. [16]. The calculation of $v_{2,a}$, v_3 , v_4 , a_2 , and d_2 requires nonvanishing nucleon momenta. Note that for the quenched theory there is no mixing with gluon operators. In the continuum limit the matrix elements $v_{2,a}$ and $v_{2,b}$ should be equal. At finite lattice spacing this provides us with a consistency check and gives information about possible lattice artifacts.

We have computed the renormalization constants for our operators in the quenched approximation for Wilson fermions in perturbation theory to one-loop order. For this task we have developed packages of computer algebraic programs using MATHEMATICA and MAPLE to such a level that all that is

TABLE III. The renormalization constants in the quenched approximation. The errors quoted are a conservative estimate of the uncertainties in the numerical evaluation of the integrals involved. The numbers in the rightmost column represent the contribution of the continuum operators computed in the $\overline{\text{MS}}$ scheme.

$\langle \mathcal{O} \rangle$	$\gamma_{\mathcal{O}}$	$B_{\mathcal{O}}$	$Z_{\mathcal{O}}(1, g = 1.0)$	$B_{\mathcal{O}}^{\overline{\text{MS}}}$
$v_{2,a}$	$\frac{16}{3}$	-3.165(6)	1.0267(1)	$-\frac{40}{9}$
$v_{2,b}$	$\frac{16}{3}$	-1.892(6)	1.0160(1)	$-\frac{40}{9}$
v_3	$\{\}\{\}$: $\frac{25}{3}$	-19.572(10)	1.1653(1)	$-\frac{67}{9}$
	$\{\}()$: 0	0.370(10)	-0.0031(1)	
v_4	$\frac{157}{15}$	-37.16(30)	1.314(3)	$-\frac{2216}{225}$
a_0	0	15.795(3)	0.8666(0)	0
a_2	$\frac{25}{3}$	-19.560(10)	1.1652(1)	$-\frac{67}{9}$
d_2	$\frac{7}{3}$	-15.680(10)	1.1324(1)	$-\frac{13}{12}$

needed as input is to state the Feynman rules in symbolic form, both for the continuum and the lattice part of the calculation. We will summarize our results here. A detailed account of our calculation will be given elsewhere [17].

In the case of v_3 it turns out that the operator $\mathcal{O}_{\{114\}} - \frac{1}{2}(\mathcal{O}_{\{224\}} + \mathcal{O}_{\{334\}})$ mixes with the operator [16]

$$\mathcal{O}_{(114)} - \frac{1}{2}(\mathcal{O}_{(224)} + \mathcal{O}_{(334)}),$$

$$\mathcal{O}_{(\mu\mu\nu)} = \mathcal{O}_{\mu\mu\nu} + \mathcal{O}_{\mu\nu\mu} - 2\mathcal{O}_{\nu\mu\mu} \quad (21)$$

under renormalization. This operator is of mixed symmetry, is traceless, and corresponds to the representation $8^{(+)}, C = -$ as well. Thus we have

$$\mathcal{O}_{\{\}\{\}}(\mu) = Z_{\{\}\{\}}\mathcal{O}_{\{\}\{\}}(a) + Z_{\{\}()\}\mathcal{O}_{\{\}()\}(a), \quad (22)$$

where we have used a shorthand notation for the operators in Table II and Eq. (21). We write ($C_F = 4/3$)

$$Z_{\mathcal{O}}((a\mu)^2, g) = 1 - \frac{g^2}{16\pi^2} C_F [\gamma_{\mathcal{O}} \ln(a\mu) + B_{\mathcal{O}}]. \quad (23)$$

This is to be interpreted as a matrix equation in the case of v_3 . Our results for the anomalous dimensions $\gamma_{\mathcal{O}}$ and the $B_{\mathcal{O}}$'s are given in Table III for $r = 1$. The renormalization constants $Z_{v_{2,b}}$ and Z_{a_0} have been given before in the literature [18–20]. We agree with the results of these authors. In the case of v_3 the off-diagonal component of Z is negligibly small.

The structure functions do not depend on μ , but $\langle x^{n-1} \rangle$ and Δu , Δd do. In the following we shall quote our results for

$$\mu^2 = Q^2 = a^{-2}, \quad (24)$$

which eliminates the logarithms in the Wilson coefficients and renormalization constants. At our smallest quark mass, taking the nucleon mass as the scale, the inverse lattice spacing is $a^{-1} \approx 1.4$ GeV. In the chiral limit we find $a^{-1} \approx 2$ GeV. We will denote $Z_{\mathcal{O}}(1, g = 1.0)$ by $Z_{\mathcal{O}}$. The corresponding numerical values are also listed in Table III. As the Wilson coefficients are generally computed in the modified minimal subtraction ($\overline{\text{MS}}$) regularization scheme, one needs to know the renormalization constants in this scheme

too. In Table III we state the contribution of the continuum operators computed in the $\overline{\text{MS}}$ scheme. The difference of the $B_{\mathcal{O}}$'s then gives the result in the $\overline{\text{MS}}$ scheme.

The renormalization constants receive contributions from five different types of diagrams: the vertex, the leg self-energy, the leg tadpole, the operator tadpole, and the operator comb diagrams. The tadpole diagrams give by far the largest contribution to the renormalization constants. The leg tadpole contribution is the same for all operators. The operator tadpole contribution is proportional to the number of covariant derivatives and has opposite sign to the leg tadpole. Leg and operator tadpole diagrams cancel each other in v_2 . This accounts for the small values of $B_{v_{2,a}}, B_{v_{2,b}}$. In a_0 only the leg tadpole contributes. In all other cases it is the operator tadpole diagram which dominates.

IV. STRUCTURE FUNCTION RESULTS

The next step is to calculate the ratio of three- to two-point correlation functions R , as given in Eq. (13), for the operators listed in Table II. To make sure that we are computing the matrix elements of the lowest-lying state, i.e., the nucleon, we must look for plateaus in τ , the time distance of the operator from the source, for $0 \ll \tau \ll t = 13$. In Fig. 3 we show R as a function of τ for six of our operators at $\kappa = 0.153$. The ratio $R_{v_{2,b}}$ not shown here is of the same quality as $R_{v_{2,a}}$. We find in all cases that the signal is practically constant for time distances larger than two lattice spacings from the source and from the sink. For $13 \leq \tau$ the signal is practically zero as one would expect. The fit interval is taken to be $4 \leq \tau \leq 9$. The result of the fit is shown by the horizontal lines, and the errors are indicated by the dotted lines.

The renormalized operator matrix elements are obtained from the ratio R by

$$\begin{aligned} R_{v_{2,a}} &= \frac{i}{Z_{v_{2,a}}} \frac{1}{2\kappa} p_1 v_{2,a}, & R_{v_{2,b}} &= -\frac{1}{Z_{v_{2,b}}} \frac{1}{2\kappa} m_N v_{2,b}, \\ R_{v_3} &= -\frac{1}{Z_{v_3}} \frac{1}{2\kappa} p_1^2 v_3, & R_{v_4} &= \frac{1}{Z_{v_4}} \frac{1}{2\kappa} E_{p_1} p_1^2 v_4, \\ R_{a_0} &= \frac{i}{Z_{a_0}} \frac{1}{2\kappa} \frac{m_N}{2E_{p_1}} a_0, & R_{a_2} &= \frac{1}{Z_{a_2}} \frac{1}{2\kappa} \frac{1}{6} m_N p_1 a_2, \\ R_{d_2} &= \frac{1}{Z_{d_2}} \frac{1}{2\kappa} \frac{1}{3} m_N p_1 d_2. \end{aligned} \quad (25)$$

We have defined the continuum quark fields by $\sqrt{2\kappa}$ times the lattice quark fields. For the renormalization constants we take the perturbative values given in Table III. In the case of v_3 we have also computed the nucleon matrix element of the operator in Eq. (21). It turned out to be noisy and consistent with zero within an error of roughly 1/5 the magnitude of the leading symmetric contribution. Given the small off-diagonal component of the renormalization constant, we may thus safely neglect the effect of mixing. Tadpole resummation [21] would leave $Z_{v_{2,a}}, Z_{v_{2,b}}$ unchanged, while it would change the other renormalization constants by a few percent.

The exact amount depends on how it is implemented, and there is considerable freedom to do so. (It is better to compute the renormalization constants nonperturbatively [22]; that is what we are doing now [23].) The results are plotted in Figs. 4 and 5 and the numerical values are listed in Table IV. All our results are given for the proton. The distribution functions of the neutron are obtained by interchanging u and d .

We shall now discuss our results in detail. The first important observation to make is that the values of $\langle x \rangle_a$ and $\langle x \rangle_b$, which are obtained from different representations of the hypercubic group $H(4)$ (cf. Table II), are consistent with each other, within the error bars. This indicates that lattice artifacts are presumably small. A second observation is that all matrix elements show roughly a linear behavior in $1/\kappa$, i.e., in the quark mass [cf. Eq. (10)]. The lines shown in Figs. 4 and 5 are linear fits to the data. The result of the extrapolation is indicated by the solid circles and the solid box, and the numerical values of the fit are given in the last column of Table IV.

Let us concentrate on the moments of the unpolarized structure functions shown in Fig. 4 first. We see that the lowest moment ($n=2$) is practically independent of the quark mass. For growing n the moments show a stronger and stronger increase with the quark mass. For the distribution function itself this means that at small x quark mass effects are negligible, while at intermediate and large x its shape depends strongly on the magnitude of the quark mass. In the limit of large quark masses the higher moments approach the predictions of the nonrelativistic quark model. In particular we find $\langle x^{n-1} \rangle^{(u)} \approx 2 \langle x^{n-1} \rangle^{(d)}$ for all n . In the chiral limit the picture changes completely. Whereas at small x the ratio of u to d distribution is roughly two, the ratio increases rapidly for larger values of x .

We may compare our results in the chiral limit with the phenomenological valence quark distribution functions. Fit D₋ of Ref. [24] gives $\langle x \rangle^{(u)} = 0.284$, $\langle x \rangle^{(d)} = 0.108$, $\langle x^2 \rangle^{(u)} = 0.083$, $\langle x^2 \rangle^{(d)} = 0.026$, $\langle x^3 \rangle^{(u)} = 0.032$, and $\langle x^3 \rangle^{(d)} = 0.009$. Fit CTEQ3M of Ref. [25] gives $\langle x \rangle^{(u)} = 0.301$, $\langle x \rangle^{(d)} = 0.083$, $\langle x^2 \rangle^{(u)} = 0.090$, $\langle x^2 \rangle^{(d)} = 0.038$, $\langle x^3 \rangle^{(u)} = 0.036$, and $\langle x^3 \rangle^{(d)} = 0.009$. It appears that the quenched lattice results for $\langle x \rangle$ are significantly larger than the values obtained from the phenomenological valence quark distribution functions, while for $\langle x^3 \rangle$ the lattice results are smaller than the phenomenological values. This is true for both, u and d quark distributions. Thus, our calculation would predict a valence quark distribution function that is larger at small to intermediate values of x and smaller at large values of x than the phenomenological distribution functions. But this is a lame comparison because we are dealing with probabilities. Consider $\langle x \rangle$, and let the subscripts V , S , and G denote the valence quark, sea quark, and gluon contribution. Momentum conservation then demands that $\langle x \rangle_V^{(u)} + \langle x \rangle_V^{(d)} + \langle x \rangle_S + \langle x \rangle_G = 1$. In the quenched approximation $\langle x \rangle_S = 0$, so that valence quark and gluon contributions should sum up to one. If, for example, the gluon contribution is approximately equal in both cases, we would thus expect to find that the quenched quark result is noticeably larger than the valence quark contribution. A better quantity to compare is therefore the difference of u - and

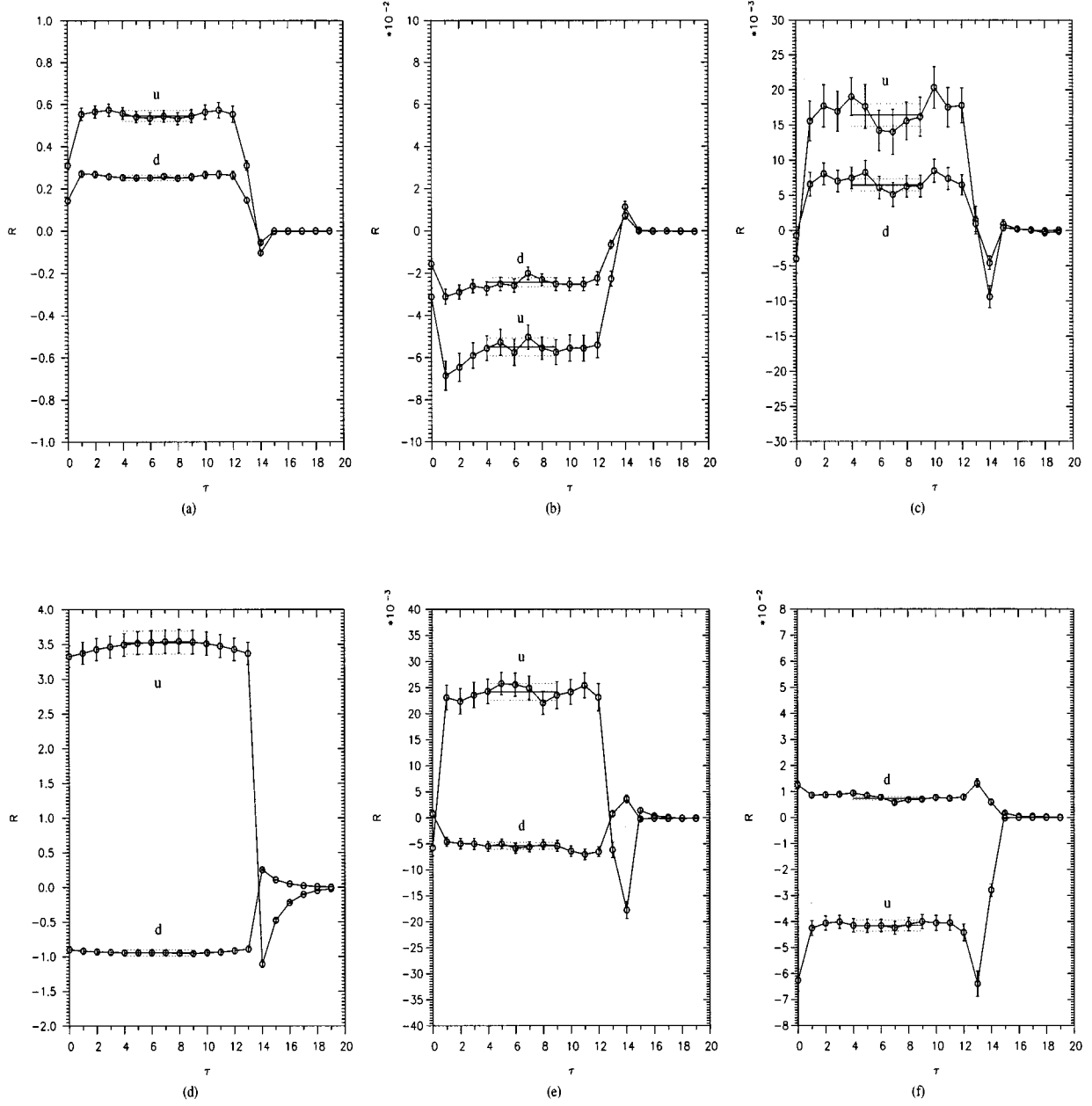


FIG. 3. The ratio R for u and d quark insertions for $\kappa=0.153$. (a) $-iR_{v_{2,d}}$, (b) R_{v_3} , (c) R_{v_4} , (d) $-iR_{a_0}$, (e) R_{a_2} , and (f) R_{d_2} . Both source and sink are smeared. The source is at $t=0$, the sink at $t=13$.

d -quark distribution functions in which the sea quark and the gluon contributions drop out. In the chiral limit we obtain $\langle x \rangle^{(u)} - \langle x \rangle^{(d)} = 0.26(4)$. This result is only one standard deviation away from the CTEQ3M result of 0.22. For the higher moments we find agreement with the phenomenological numbers within the error bars.

We shall now turn to the discussion of our results for the polarized structure functions shown in Fig. 5. Let us first focus on Δu and Δd , which in the quenched approximation determine the fraction of the proton spin that is carried by the valence quarks. Sea quark effects may be neglected for heavy quarks, and they drop out in the difference $\Delta u - \Delta d$. In the chiral limit we obtain

$$\Delta u - \Delta d \equiv g_A = 1.07(9). \quad (26)$$

This is to be compared with the experimental value of the axial vector coupling constant $g_A = 1.26$. If we add the sea quark contribution to our results — a recent lattice calculation [27] finds $\Delta \bar{u} = \Delta \bar{d} = -0.14(5)$, $\Delta \bar{s} = -0.13(4)$ using perturbative renormalization factors—we find good agreement with a recent phenomenological fit of the individual contributions [26] except for Δu . For the total quark spin contribution to the nucleon spin we would furthermore obtain $\Delta \Sigma = 0.18(11)$, in agreement with the result of a full QCD calculation [28], i.e., including dynamical quarks. For heavy quark masses we find $\Delta u \approx 1$ and $\Delta d \approx -1/4$, in good agreement with the three-quark model [29].

By comparing the moments $a_0 = 2\Delta q$ and a_2 with those of the unpolarized structure functions we find that in the chiral limit g_1 is less singular than F_1 as x goes to zero. This

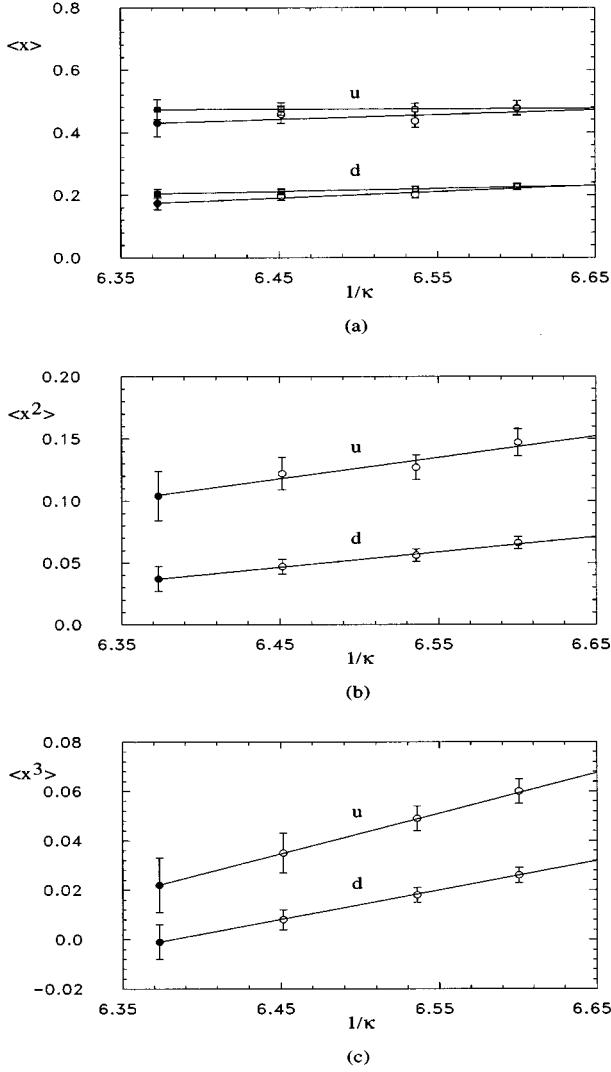


FIG. 4. The moments of the unpolarized proton structure functions as a function of $1/\kappa$, together with a linear fit to the data. The solid symbols indicate the extrapolation to the chiral limit. In (a) the circles refer to $\langle x \rangle_a$, boxes to $\langle x \rangle_b$.

is also what one finds experimentally [30]. In the limit of large quark masses, on the other hand, it seems that g_1 is proportional to F_1 .

If we combine our results with the perturbatively known [31] Wilson coefficients we can compute the moments of g_1 . In the chiral limit we obtain, for the lowest moment,

$$\int_0^1 dx g_1(x, Q^2) = \begin{cases} 0.166(16) & \text{proton,} \\ -0.008(09) & \text{neutron.} \end{cases} \quad (27)$$

Recall that $Q^2 \approx 4 \text{ GeV}^2$. For the difference of proton and neutron structure functions we find

$$\int_0^1 dx [g_1^p(x, Q^2) - g_1^n(x, Q^2)] = 0.174(25). \quad (28)$$

Our result is in good agreement with the phenomenological analysis [26,30]. In the higher moments of g_1 sea quark effects should not play any role anymore. In the chiral limit we obtain

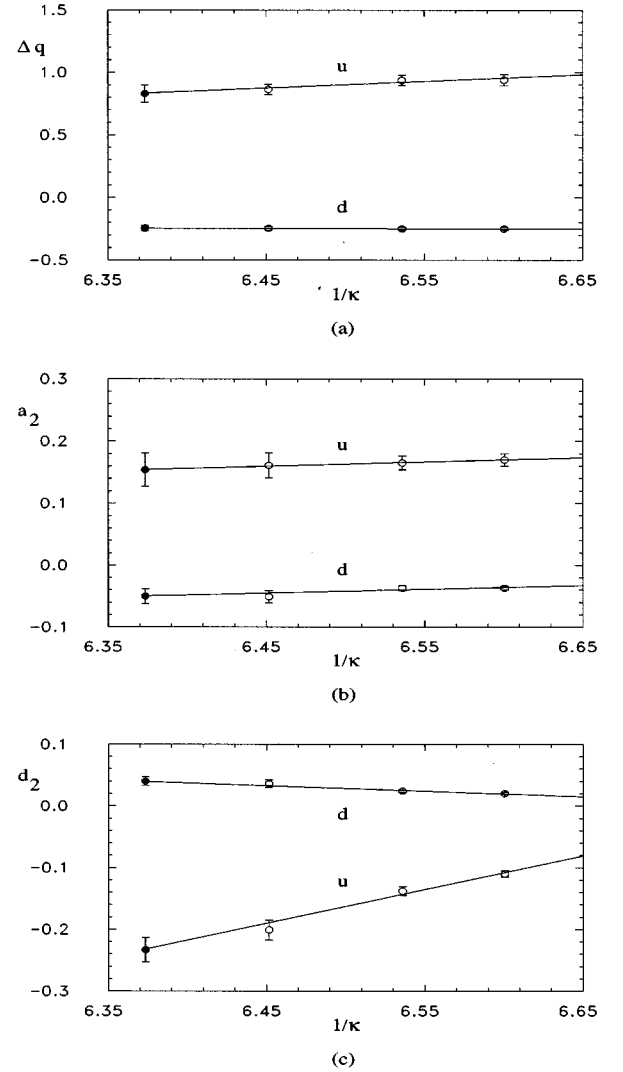


FIG. 5. The moments of the polarized proton structure functions as a function of $1/\kappa$, together with a linear fit to the data. The solid symbols indicate the extrapolation to the chiral limit.

$$\int_0^1 dx x^2 g_1(x, Q^2) = \begin{cases} 0.0150(32) & \text{proton,} \\ -0.0012(20) & \text{neutron.} \end{cases} \quad (29)$$

Here we have converted the renormalization constants to the $\overline{\text{MS}}$ scheme, because the Wilson coefficients were computed in this scheme too. This result is consistent with experiment [32].

Let us finally discuss the structure function g_2 . From Fig. 5(c) we read off that the twist-three contribution d_2 is strongly mass dependent. While d_2 approaches zero in the heavy quark limit, for both u and d quark insertion, it is of the same order of magnitude as its twist-two counterpart a_2 for small quark masses. In the chiral limit we obtain

$$\int_0^1 dx x^2 g_2(x, Q^2) = \begin{cases} -0.0161(16) - 0.0100(22) = -0.0261(38) & \text{proton,} \\ -0.0013(09) + 0.0009(13) = -0.0004(22) & \text{neutron.} \end{cases} \quad (30)$$

TABLE IV. Structure function results for the proton. All numbers refer to the momentum subtraction scheme.

Observable	κ			
	0.1515	0.153	0.155	$\kappa_c=0.1569$
$\langle x \rangle_a^{(u)}$	0.477(23)	0.436(20)	0.457(28)	0.430(43)
$\langle x \rangle_b^{(u)}$	0.478(22)	0.473(20)	0.475(20)	0.473(32)
$\langle x \rangle_{av}^{(u)}$	0.478(16)	0.455(14)	0.466(16)	0.452(26)
$\langle x \rangle_a^{(d)}$	0.226(11)	0.201(10)	0.195(12)	0.174(20)
$\langle x \rangle_b^{(d)}$	0.226(10)	0.219(09)	0.211(09)	0.204(15)
$\langle x \rangle_{av}^{(d)}$	0.226(08)	0.210(07)	0.203(07)	0.189(12)
$\langle x^2 \rangle^{(u)}$	0.147(11)	0.127(10)	0.122(13)	0.104(20)
$\langle x^2 \rangle^{(d)}$	0.066(05)	0.056(05)	0.047(06)	0.037(10)
$\langle x^3 \rangle^{(u)}$	0.060(05)	0.049(05)	0.035(08)	0.022(11)
$\langle x^3 \rangle^{(d)}$	0.026(03)	0.018(03)	0.008(04)	-0.001(07)
Δu	0.938(45)	0.935(44)	0.863(43)	0.830(70)
Δd	-0.250(12)	-0.250(12)	-0.246(14)	-0.244(22)
$a_2^{(u)}$	0.170(10)	0.165(11)	0.161(20)	0.154(27)
$a_2^{(d)}$	-0.037(03)	-0.037(04)	-0.051(10)	-0.050(12)
$d_2^{(u)}$	-0.110(05)	-0.138(07)	-0.201(16)	-0.233(20)
$d_2^{(d)}$	0.020(02)	0.024(02)	0.036(06)	0.040(07)

As before, Wilson coefficients [31] and renormalization constants are consistently computed in the $\overline{\text{MS}}$ scheme. In Eq. (30) the first number comes from d_2 , while the second number comes from a_2 [cf. Eq. (6)]. We see that the twist-three operator provides the dominant contribution. The Wandzura-Wilczek description of g_2 [5] is a valid approximation for large quark masses, but for light quark masses it is definitely not. Our results seem to be in disagreement with recent estimates based on sum rules [33], which suggest that for the proton d_2 is very small. Because the gluon contribution, which we have neglected, may be large, one should perhaps only compare the difference of proton and neutron structure functions as in the previous cases.

V. CONCLUSION

We have presented results of a calculation of the lower moments of the polarized and unpolarized deep-inelastic

structure functions of the nucleon. The calculation has been performed in the quenched approximation, where sea quark effects are neglected, and it was done for three different quark masses. This allowed us to extrapolate our results to the chiral limit.

The valence quark distributions that we have obtained differ somewhat from the phenomenological ones [24]. One explanation could be that at smaller values of Q^2 higher twist contributions are non-negligible, which have not been included in the phenomenological analysis. We plan to investigate this possibility in the future. Our results for the polarized structure functions are consistent with experiment, as far as data exist. A surprise was that the twist-three operator contributed so much to g_2 .

It was interesting to see how the results varied with the quark mass. At large quark masses our results agree largely with what one would expect on the basis of the quark model. For small quark masses there are, however, significant changes.

With the (raw) lattice data being relatively accurate now, the calculation of the renormalization constants has become a major issue. So far we have computed the renormalization constants in perturbation theory to one-loop order. We hope to do better in the near future [23].

The renormalization constant for v_3 has independently been computed by the Rome group [34]. We have compared our results with theirs at intermediate stages of the calculation, and they agreed. These authors use a slightly different basis of operators from ours though.

ACKNOWLEDGMENTS

This work was supported in part by the Deutsche Forschungsgemeinschaft. The numerical calculations were performed on the Quadrics parallel computers at Bielefeld University and at DESY (Zeuthen). We wish to thank both institutions for their support and in particular the system managers M. Plagge and H. Simma for their help. We furthermore would like to thank S. Capitani and G. Rossi for discussions on the problem of perturbative renormalization.

[1] J. Ashman *et al.*, Phys. Lett. B **206** 364 (1988); Nucl. Phys. **B328**, 1 (1989).
[2] R. L. Jaffe, Comments Nucl. Part. Phys. **19**, 239 (1990).
[3] M. Göckeler, R. Horsley, E.-M. Ilgenfritz, H. Perlt, P. Rakow, G. Schierholz, and A. Schiller, in *Lattice '94*, Proceedings of the International Symposium, Bielefeld, Germany, edited by F. Karsch *et al.* [Nucl. Phys. B (Proc. Suppl.) **42**, 337 (1995)].
[4] G. Martinelli and C. T. Sachrajda, Nucl. Phys. **B316**, 355 (1989); G. Martinelli, in *Lattice '88*, Proceedings of the International Symposium, Batavia, Illinois, edited by A. S. Kronfeld and P.B. Mackenzie [Nucl. Phys. B (Proc. Suppl.) **9**, 134 (1989)].
[5] S. Wandzura and F. Wilczek, Phys. Lett. **72B**, 195 (1977).
[6] R. L. Jaffe and X. Ji, Phys. Rev. D **43**, 724 (1991).

[7] M. Creutz, Phys. Rev. D **36**, 516 (1987).
[8] C. R. Allton *et al.*, Phys. Rev. D **47**, 5128 (1993).
[9] S. G. Güsken, in *Lattice '89*, Proceedings of the International Symposium, Capri, Italy, edited by R. Petronzio *et al.* [Nucl. Phys. B (Proc. Suppl.) **17**, 361 (1990)]; C. Alexandrou, S. G. Güsken, F. Jegerlehner, K. Schilling, and R. Sommer, Nucl. Phys. **B414**, 815 (1994).
[10] S. Cabasino *et al.*, Phys. Lett. B **258**, 195 (1991).
[11] T. Bhattacharya and R. Gupta, in *Lattice '93*, Proceedings of the International Symposium, Dallas, Texas, edited by T. Draper *et al.* [Nucl. Phys. B (Proc. Suppl.) **34**, 341 (1994)].
[12] Y. Iwasaki, K. Kanaya, S. Sakai, T. Yoshié, T. Hoshino, and T. Shirakawa, in *Lattice '93* [11], p. 354.
[13] C. Bernard, T. Blum, C. DeTar, S. Gottlieb, U. M. Heller, J.

- Hetrick, K. Rummukainen, R. Sugar, D. Toussaint, and M. Wingate, Indiana Report No. IUHET-315, 1995 (hep-lat/9509076) (unpublished).
- [14] M. Baake, B. Gemünden, and R. Oedingen, *J. Math. Phys.* **23**, 944 (1982), **23**, 2595(E) (1982).
- [15] J. Mandula, G. Zweig, and J. Govaerts, *Nucl. Phys.* **B228**, 109 (1983).
- [16] M. Göckeler, R. Horsley, E.-M. Ilgenfritz, H. Perlt, P. Rakow, G. Schierholz, and A. Schiller (in preparation).
- [17] M. Göckeler, R. Horsley, E.-M. Ilgenfritz, H. Perlt, P. Rakow, G. Schierholz, and A. Schiller (in preparation).
- [18] G. Martinelli and Y. C. Zhang, *Phys. Lett.* **123B** 433 (1983).
- [19] G. Martinelli and C. T. Sachrajda, *Nucl. Phys.* **B306**, 865 (1988).
- [20] S. Capitani and G. Rossi, *Nucl. Phys.* **B433**, 351 (1995).
- [21] G. P. Lepage and P. B. Mackenzie, *Phys. Rev. D* **48**, 2250 (1993).
- [22] G. Martinelli, C. Pittori, C. T. Sachrajda, M. Testa, and A. Vladikas, *Nucl. Phys.* **B445**, 81 (1995).
- [23] M. Göckeler, R. Horsley, E.-M. Ilgenfritz, H. Oelrich, H. Perlt, P. Rakow, G. Schierholz, and A. Schiller, DESY Report No. DESY 95-179, 1995 (hep-lat/9510017) (unpublished).
- [24] A. D. Martin, W. J. Stirling, and R. G. Roberts, *Phys. Rev. D* **47**, 867 (1993).
- [25] H. L. Lai, J. Botts, J. Huston, J. G. Morfin, J. F. Owens, J. W. Qiu, W. K. Tung, and H. Weerts, *Phys. Rev. D* **51**, 4763 (1995).
- [26] J. Ellis and M. Karliner, *Phys. Lett. B* **341**, 397 (1995).
- [27] M. Fukugita, Y. Kuramashi, M. Okawa, and A. Ukawa, KEK Report No. 94-173 1994 (unpublished); S. J. Dong, J.-F. Lagaë, and K.-F. Liu, *Phys. Rev. Lett.* **75**, 2096 (1995).
- [28] R. Altmeyer, M. Göckeler, R. Horsley, E. Laermann, and G. Schierholz, *Phys. Rev. D* **49**, R3087 (1994).
- [29] S. J. Brodsky and F. Schlumpf, *Phys. Lett. B* **329**, 111 (1994); S. J. Brodsky, in *Spin Structure in High Energy Processes*, Proceedings of the XXI SLAC Summer Institute on Particle Physics, Stanford, California, 1993, edited by L. DePorcel and C. Dunwoodie (SLAC Report No. 444, Stanford, 1994), p. 81.
- [30] D. Adams *et al.*, *Phys. Lett. B* **329**, 399 (1994); K. Abe *et al.*, *Phys. Rev. Lett.* **74**, 346 (1995).
- [31] J. Kodaira, S. Matsuda, T. Muta, T. Uematsu, and K. Sasaki, *Phys. Rev. D* **20**, 627 (1979); R. Mertig and W. L. van Neerven, *Z. Phys. C* **60**, 489 (1993).
- [32] E. Hughes, in *Spin Structure in High Energy Processes* [29], p. 129.
- [33] I. I. Balitsky, V. M. Braun, and A. V. Kolesnichenko, *Phys. Lett. B* **242**, 245 (1990); E. Stein, P. Górnicki, L. Mankiewicz, A. Schäfer, and W. Greiner, *ibid.* **343**, 369 (1995).
- [34] G. Beccarini, M. Bianchi, S. Capitani, and G. Rossi, *Nucl. Phys.* **B456** 271 (1995).